Midlatitude Atmosphere–Ocean Interaction during El Niño. Part I: The North Pacific Ocean

MICHAEL A. ALEXANDER

Department of Meteorology and Center for Climatic Research, University of Wisconsin—Madison, Madison, Wisconsin

(Manuscript received 3 May 1991, in final form 2 January 1992)

ABSTRACT

Atmosphere–ocean modeling experiments are used to investigate the formation of sea surface temperature (SST) anomalies in the North Pacific Ocean during fall and winter of the El Niño year. Experiments in which the NCAR Community Climate Model (CCM) surface fields are used to force a mixed-layer ocean model in the North Pacific (no air–sea feedback) are compared to simulations in which the CCM and North Pacific Ocean model are coupled. Anomalies in the atmosphere and the North Pacific Ocean during El Niño are obtained from the difference between simulations with and without prescribed warm SST anomalies in the tropical Pacific. In both the forced and coupled experiments, the anomaly pattern resembles a composite of the actual SST anomaly field during El Niño: warm SSTs develop along the coast of North America and cold SSTs form in the central Pacific. In the coupled simulations, air–sea interaction results in a 25% to 50% reduction in the magnitude of the SST and mixed-layer depth anomalies, resulting in more realistic SST fields. Coupling also decreases the SST anomaly variance; as a result, the anomaly centers remain statistically significant even though the magnitude of the anomalies is reduced.

Three additional sensitivity studies indicate that air–sea feedback and entrainment act to damp SST anomalies while Ekman pumping has a negligible effect on mixed-layer depth and SST anomalies in midlatitudes.

1. Introduction

Air–sea interaction appears to play a key role in a wide range of phenomena, from the development of oceanic storms to the global-scale changes associated with El Niño and the Southern Oscillation. The exchange of energy between the atmosphere and ocean is controlled by the near-surface wind, the temperature and humidity, and the sea surface temperature (SST). In midlatitudes, departures in the SST from the seasonal mean strongly depend on air–sea interactions (Gill and Niiler 1973; Frankignoul 1985), which results in a close association between the large-scale SST and atmospheric anomaly patterns (Namias 1973; Cayan 1980). Lag-correlation analyses (Davis 1976; Lanzante 1984; Wallace and Jiang 1987), stochastic models of SST anomaly development (Frankignoul and Hasselman 1977; Frankignoul and Reynolds 1983), and coupled atmosphere–ocean model simulations (Salmon and Hendershott 1976) indicate that the atmosphere tends to drive the ocean in the extratropics. However, the developing ocean anomalies may feed back on the atmosphere. Several studies have indicated that in certain seasons midlatitude SSTs influence the evolution of the atmospheric circulation (Davis 1978; Walsh and Richman 1981; Palmer and Sun 1985; Pitcher et al. 1988; Wallace et al. 1990; Lau and Nath 1990).

Anomalous atmospheric forcing can cause SST anomalies to form by surface energy fluxes, vertical mixing due to turbulence, and wind-driven vertical and horizontal motions associated with Ekman pumping and transport. The influence of Ekman pumping and transport in the open ocean on the development of SST anomalies is somewhat uncertain. Emery (1976) concluded that Ekman pumping changes the thermal structure of the upper ocean, while White (1978), White et al. (1980), and Haney et al. (1983) indicate that it has a negligible impact on large-scale SST anomalies. The case studies of Namias (1959, 1965, 1972) and Clark (1972) suggest that meridional temperature advection by anomalous currents plays an important role in the formation of SST anomalies. Model simulations indicate that along the polar front, at approximately 40°N in the central and west Pacific, anomalous Ekman transport can influence ocean temperatures (Haney 1980; Luksch et al. 1990). However, SSTs appear primarily to be controlled by surface fluxes and the entrainment of deeper water into the mixed layer in the midlatitude oceans (Frankignoul and Reynolds 1983; Frankignoul 1985; Haney 1985).

The most prominent SST anomaly patterns in the North Pacific are nearly basinwide, as indicated by the empirical orthogonal function (EOF) analyses of Weare et al. (1976) and Davis (1976). The dominant

Corresponding author address: Dr. Michael A. Alexander, University of Colorado, CIRES, Campus Box 449, Boulder, CO 80309-0449.

mode of variability, the first EOF, has a zonally elongated center that extends across the Pacific at ~35°N and a center of opposite sign in the Gulf of Alaska. This pattern often occurs during El Niño when the water is anomalously warm in the northeast Pacific and cold in the central Pacific, while the same pattern but with opposite sign tends to occur during La Niña (Weare et al. 1976; Pan and Oort 1983, 1990; Emery and Hamilton 1985). A composite of the observed difference between North Pacific SSTs during El Niño and La Niña events in boreal winter is shown in Fig. 1.

The correlation analysis of Wright (1983) suggests that changes in the Southern Oscillation, a dipole in the sea level pressure that spans the tropical Pacific and is closely associated with the El Niño/La Niña cycle, lead SST anomalies in the North Pacific by one to two months. The atmosphere, rather than the ocean, may communicate changes in the tropical Pacific to the North Pacific as most large-scale dynamical processes in the ocean are relatively slow. The major exception is Kelvin waves, which can travel large distances on seasonal time scales. Coastal Kelvin waves, forced by oceanic conditions in the equatorial Pacific, influence SSTs near North America during El Niño (Enfield and Allen 1980; Johnson and O'Brien 1990). However, these waves are confined to a narrow region near the shore and therefore do not appear to explain the basinwide SST anomaly pattern that occurs concurrently with El Niño events.

Several recent observational studies, including Wagner (1984), Emery and Hamilton (1985), Hanawa et al. (1989), and Luksch et al. (1990), have found evidence that changes in atmospheric circulation during El Niño could lead to the formation of SST anomalies in the North Pacific. As first noted by Bjerknes (1966, 1969), the Aleutian Low often intensifies and shifts southward during El Niño events. The resulting strengthened surface westerlies in the central Pacific and southerly winds in the eastern Pacific alter the surface fluxes, vertical mixing, and ocean currents in a manner that is consistent with the observed SST anomalies that form during El Niño (Mysak 1986).

The influence of El Niño–induced atmospheric changes on the North Pacific Ocean was recently examined in the modeling experiments of Alexander (1990; hereafter MAA). In that study, a mixed-layer model of the North Pacific Ocean was forced with surface energy flux and wind-stress fields from the NCAR Community Climate Model (CCM), an atmospheric general circulation model (GCM). The flux fields were taken from two sets of experiments with different SST fields prescribed in the tropical Pacific, one with warm SSTs representing El Niño conditions and the other with climatological SSTs. The simulated midlatitude SST anomalies, obtained from the difference between the two sets, were realistic, with positive (negative) anomalies in the northeast (central) Pacific. The SST anomalies were caused by changes in the surface energy fluxes as a result of a strengthening and southeast displacement of the Aleutian Low in late fall and winter.

In the present study, we expand on the findings of MAA by using two sets of model analyses to address how feedback processes influence the SST anomalies that develop in the North Pacific during El Niño. In the first set, three sensitivity tests are performed to investigate the effects of surface energy fluxes, entrainment, and Ekman pumping on the development of ocean anomalies. In the second set, anomalies that form in coupled CCM/North Pacific Ocean model simu-

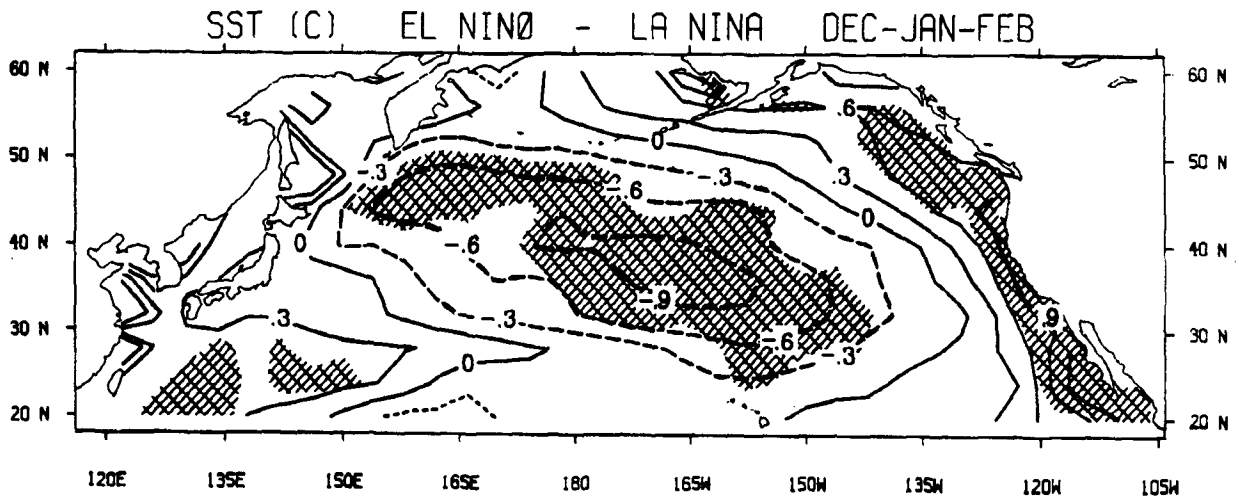

FIG. 1. The observed difference in sea surface temperature (°C) between El Niño and La Niña December–January–February periods. The SST values are from 1946 to 1989 in the COADS dataset, which contains nine El Niño events (1951–52, 53, 57, 65, 69, 72, 76, 82, 86) and nine La Niña events (1949–50, 55, 62, 64, 67, 70, 73, 75, 88). Shaded areas indicate where the t statistic of the SST differences are significant at the 5% level.

lations are compared to similar uncoupled simulations in order to examine the influence of air–sea interaction on the formation of ocean anomalies. As in MAA, anomalies are obtained from the difference between simulations with either climatological or idealized El Niño SSTs specified in the tropical Pacific. The design of the ocean–atmosphere model system and a description of the numerical experiments are given in sections 2 and 3, respectively. The results from the three sensitivity studies are described in section 4 followed by the air–sea interaction analysis in section 5. The effects of the developing North Pacific SST anomalies on the atmosphere are discussed in Alexander (1992), Part II of this study.

2. The design of the ocean–atmosphere model system

A series of ocean–atmosphere simulations are used to investigate the development of anomalies in the North Pacific during El Niño. The ocean configuration (section 2a) consists of a mixed-layer model in the North Pacific and prescribed SSTs over the rest of the ocean. The North Pacific Ocean model (section 2b) and the CCM (section 2c) are connected via surface fluxes plus a flux correction (section 2d). Three different methods are used to compute the surface fluxes that connect the CCM to the North Pacific Ocean model (section 2e).

a. Ocean configuration

The ocean is represented by a mixed-layer model between 20°N and 60°N in the Pacific Ocean, while SSTs are prescribed over the remainder of the global oceans. The prescribed ocean temperatures between 20°N and 30°S in the Pacific are given by either (i) SSTs associated with El Niño or (ii) climatological SSTs. Climatological SSTs and sea-ice location are always specified over the rest of the world's oceans. The configuration of the ocean model/prescribed SST field including the prescribed El Niño SST anomalies (i–ii) in the tropical Pacific are shown in Fig. 2.

The prescribed climatological SST and sea-ice fields, obtained from the analysis of Alexander and Mobley (1976), are updated daily and go through the same seasonal cycle in all of the model simulations. In the "El Niño" simulations, prescribed SST anomalies are added to the climatological SSTs in the tropical Pacific. Following Aragão (1986), a cubic spline is used to interpolate the three-month average SST anomalies from the El Niño composite of Rasmusson and Carpenter (1982) to daily anomaly values. The anomalies are then doubled to be more representative of a single strong El Niño event and to ensure a reasonably strong atmospheric response (Aragão 1986; Blackmon et al. 1983). The prescribed SST anomalies in the tropical Pacific evolve identically in all of the El Niño simulations. In the transition and mature phases of El Niño, which occur during boreal fall and winter, positive SST anomalies cover most of the tropical Pacific (Fig. 2).

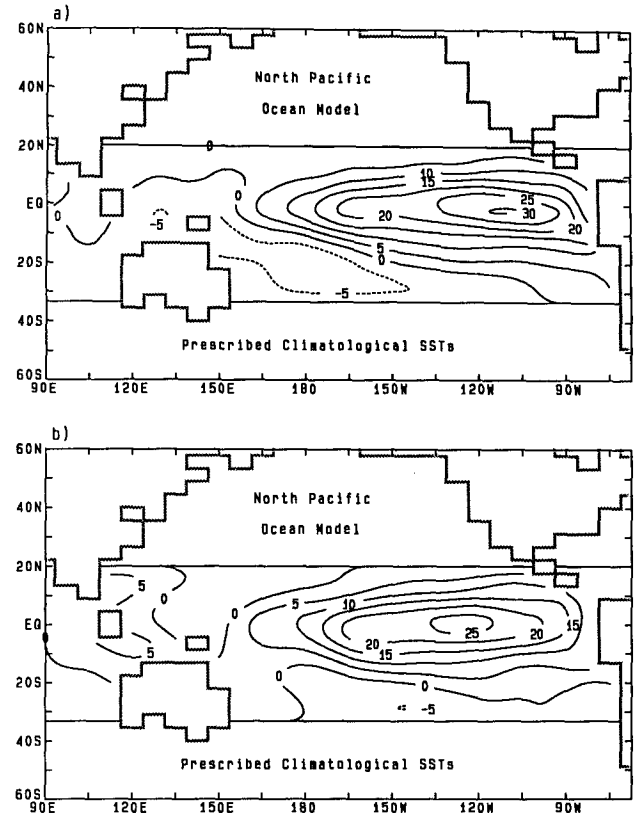

FIG. 2. The domain of the North Pacific Ocean model, prescribed climatological SSTs, and the values of the prescribed SST anomalies (°C × 10) associated with El Niño in the tropical Pacific. The anomalies are obtained by doubling the Rasmusson and Carpenter (1982) composite. The anomaly fields are presented for the transition and mature phases of El Niño that occur in Northern Hemisphere (a) September–October–November (SON) and (b) December–January–February (DJF).

b. The North Pacific Ocean model

The North Pacific Ocean model consists of a grid of independent-column models. Vertical processes including surface energy fluxes, penetrating solar radiation, molecular diffusion, entrainment, and Ekman pumping are represented in each column, but there is no horizontal communication between columns. The ocean model and CCM grids are collocated. The column model consists of a joint mixed-layer/convective-diffusive parameterization.

In mixed-layer models it assumed that a uniform surface layer exists a priori with a discontinuity in temperature (and/or salinity) at the base of the layer. Integrating the temperature tendency equation over the mixed-layer depth yields

$$\frac{\partial T_m}{\partial t} = \frac{w_e}{h}(T_b - T_m) + \frac{Q_0 - Q_b}{\rho_r c_p h} + \frac{\upsilon_H}{h}\frac{(T_b - T_m)}{\Delta h} \tag{1}$$

where T is the temperature, t the time, w_e the entrainment velocity, h the mixed-layer depth, ρ_r the reference density, c_p the specific heat of seawater, and Q_0 the net downward surface energy flux (discussed further in section 2d). Subscripts m and b denote the mixed layer and the region just beneath the mixed layer, respectively. The three terms on the right-hand side of Eq. (1) represent the effects of entrainment, surface fluxes, and molecular diffusion. Diffusion that helps to stabilize the model under extreme conditions is highly parameterized: Δh, the thickness of the pycnocline, and the υ_H diffusion coefficient for heat are assumed to be constant.

The flux at the base of the mixed layer is assumed to have the form

$$Q_b = Q_{sw}(1 - R)\exp(-\gamma h) \tag{2}$$

where Q_{sw} is the solar radiation flux at the surface, R is the percentage of sunlight absorbed in the upper few meters of the ocean, and γ is the attenuation coefficient. The assigned values of R and γ, which depend on optical water type, are obtained from Paulson and Simpson (1977) using the water-type values given by Simonot and Le Treut (1986).

Following Niiler and Kraus (1977) entrainment can be expressed as

$$w_e = \frac{2mu_*^3 + nhB_0 + \left(h - \frac{2}{\gamma}\right)\frac{g\alpha}{\rho_r c_p}(1 - R)Q_{sw}}{(\rho_b - \rho_m) - s|\mathbf{v}_m|^2} \tag{3}$$

where

$$B_0 = -\frac{g}{\rho_r}\left\{\frac{\alpha}{c_p}(Q_0 - (1 - R)Q_{sw}) + \beta S_m(P - E)\right\}, \tag{4}$$

$u_* = (|\tau|/\rho_r)^{1/2}$ is the friction velocity, τ the surface wind stress, $\mathbf{v}$ the local wind-driven velocity, g the acceleration due to gravity, S the salinity, E the evaporation rate, P the precipitation rate, and α and β are the expansion coefficients for temperature and salinity. Here S_m and $\mathbf{v}_m$ are prognostic model variables; the former is calculated using the salt conservation equation, and the latter is obtained from the simplified momentum equations of Pollard and Millard (1970). The density values in Eq. (3) are computed from the international equation of state for seawater neglecting pressure effects. The mixing efficiency factors, m, n, and s, scale the amount of entrainment due to mechanical stirring, convection, and shear-induced turbulence. A wide range of values for all three factors have been reported in the literature; we use the values obtained by Davis et al. (1981), $m = 0.39$, $s = 0.48$, and $n = 0.17$ ($n = 1.0$) when $B_0 < 0$ ($B_0 \geq 0$). Simulations with the North Pacific Ocean model indicate that the monthly averaged mixed-layer variables are not very sensitive to the choice of these parameters.

Away from the equator or coastal boundaries, under steady conditions, Ekman pumping can be expressed by

$$w_{ek} = \frac{1}{\rho_r}\nabla \times \left(\frac{\tau}{f}\right), \tag{5}$$

assuming that density is constant and that the wind-driven ocean currents are confined to the mixed layer. The Coriolis parameter, f, is a function of latitude. Ekman pumping is treated as a local phenomenon; that is, the implied horizontal convergence or divergence is assumed to occur within that grid volume and does not influence other grid points. Away from coastal areas, Ekman pumping mainly occurs within eddies in the extratropical oceans that are typically 30 to 100 km across (Frankignoul 1985), an order of magnitude smaller than the grid scale. An alternative view is that Ekman pumping vertically stretches the mixed layer, which excites baroclinic Rossby waves. In midlatitudes these waves move very slowly; for example, at 45°N the first baroclinic Rossby mode travels about 150 km in 100 days. Thus, this simplification of the effects of Ekman pumping appears to be reasonable for large spatial scales and intra-annual time scales.

Mixed-layer deepening is associated with entrainment modified by Ekman pumping and is given by

$$\frac{\partial h}{\partial t} = w_e - w_{ek}. \tag{6}$$

The mixed layer re-forms closer to the surface when surface heat and salinity fluxes act to increase the buoyancy of the mixed layer, and the turbulence due to wind stirring cannot overcome this stabilizing effect. Under these conditions h is obtained as a diagnostic by using Eq. (3) with w_e set to zero and then including the change in h over one time step due to Ekman pumping. In accordance with observed mixed-layer depths and in the absence of stirring due to surface waves, h is constrained to be greater than 10 m.

The mixed-layer model is strapped to a convective–diffusive (C–D) model using a modified version of the empirical formulation described by Heald and Kim (1979). The strapping procedure, described in the Appendix, provides estimates of T_b by conserving heat between the two model systems (Fig. 3). Both models are integrated using a 24-h time step. There are two processes that operate in the C–D model: convective adjustment and constant vertical diffusion; w_{ek} is not included in this model. Temperature and salinity are calculated in the C–D model for three layers that begin at the ocean surface and are 40, 80, and 120 m thick, respectively. The temperature is prescribed in an ad-

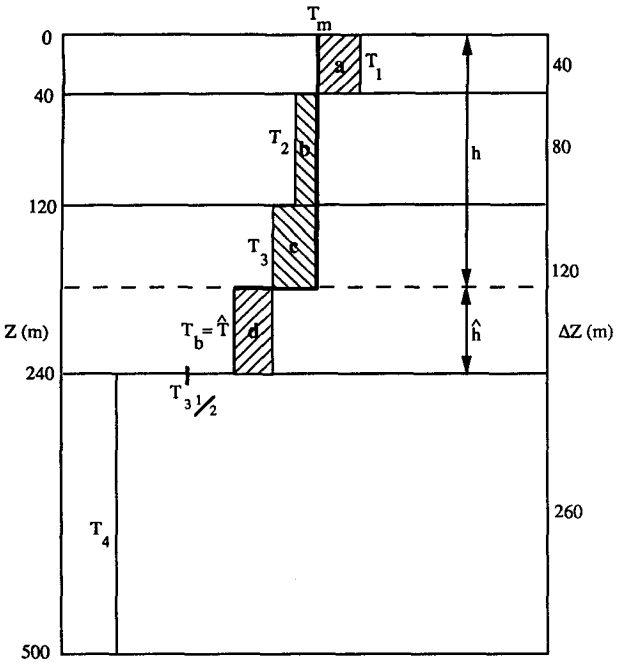

FIG. 3. The temperature of the mixed layer, T_m, and convective–diffusive model layers $T_{1,2,3,4}$ where Z (m) is the depth, ΔZ the layer thickness, and h is the depth of the mixed layer. The temperature beneath the mixed layer, T_b, and $\hat{T}$, the temperature of layer $\hat{h}$, are obtained by conserving heat in the two models, resulting in areas a + d = b + c. T_b is constrained to be greater than $T_{L+1/2}$, the average of $T_L + T_{L+1}$, where L is the layer that contains h. Adapted from Heald and Kim (1979).

ditional 260-m-thick layer in order to compute the diffusion at the bottom of the third layer.

c. *The CCM*

The CCM (version 0A, described by Washington 1982) is a 9-layer, sigma-coordinate, primitive equation GCM. It is a spectral model with rhomboidal truncation at wavenumber 15 corresponding to a horizontal resolution of approximately 4.45° latitude by 7.5° longitude. The model includes interactive clouds and radiative processes. The seasonal-cycle version of the model is described by Chervin (1986). The surface temperatures of land and sea ice are determined by solving the local heat-balance equation; other boundary conditions, such as the surface moisture and albedo, are parameterized. The CCM has simulated the large-scale circulation during January and July reasonably well (Pitcher et al. 1983) and has reproduced the basic features of the atmospheric response to tropical SST anomalies (Blackmon et al. 1983; Geisler et al. 1985; Aragão 1986).

d. *Surface fluxes and flux corrections*

The net surface energy flux into the ocean is given by

$$Q_0 = Q_{sw} - Q_{lw} - Q_{sh} - Q_{lh} \tag{7}$$

where Q_{lw} is the upward longwave radiation and Q_{sh} and Q_{lh} the upward sensible and latent heat flux, respectively. The net surface radiation depends on the fractional cloud cover, amount of atmospheric water vapor, and the surface temperature and albedo. The fluxes Q_{sh} and Q_{lh} are computed using bulk aerodynamic formulas,

$$Q_{sh} = \rho_a c_{pa} C_D |U| (T_o - T_a), \tag{8}$$

$$Q_{lh} = \rho_a L_v C_D |U| (q_s - q_a), \tag{9}$$

where U is the wind speed, c_{pa} the specific heat of air, q the specific humidity, L_v the latent heat of vaporization, and C_D is a constant drag coefficient. Subscripts a, o, and s denote the atmosphere, ocean, and saturation value (a function of T_o), respectively. The wind speed, temperature, and humidity values used in (8) and (9) are obtained from the lowest CCM layer (σ = 0.991) located approximately 100 m above the surface. The surface fluxes of momentum (τ) and freshwater (P–E) are also obtained from the CCM.

Errors in the atmospheric forcing and the absence of important terms in the ocean model cause the simulated ocean temperatures to drift from the observed climate. Sausen et al. (1988) and Manabe and Stouffer (1988) found that model drift affects the simulated climate sensitivity and that it was necessary to apply surface flux corrections in order to maintain a reasonable model climatology. The procedure used to calculate the correction values (described in MAA) involves forcing the predicted T_m values to match the observed SSTs prescribed in the climatological CCM integrations. The corrections vary in space and time, but the same set of corrections are used to adjust the atmosphere to ocean fluxes in all of the integrations. At some locations the correction values are of the same order of magnitude as the fluxes, suggesting that significant improvements can be made in both the atmosphere and ocean models.

e. *Atmosphere–ocean coupling*

Three methods are used to connect the CCM to the North Pacific Ocean model as depicted in Fig. 4:

1) *uncoupled or one-way forced,* in which the ocean is driven by CCM surface fluxes computed using prescribed climatological SSTs;
2) *partially coupled,* in which the CCM wind, temperature, and humidity values used to compute the surface forcing are the same as in method 1), but the surface fluxes are calculated using the mixed-layer temperatures from the ocean model (i.e., $T_o = T_m$);
3) *fully coupled,* where the air–sea fluxes respond to changes in both the atmospheric variables and the ocean mixed-layer temperature.

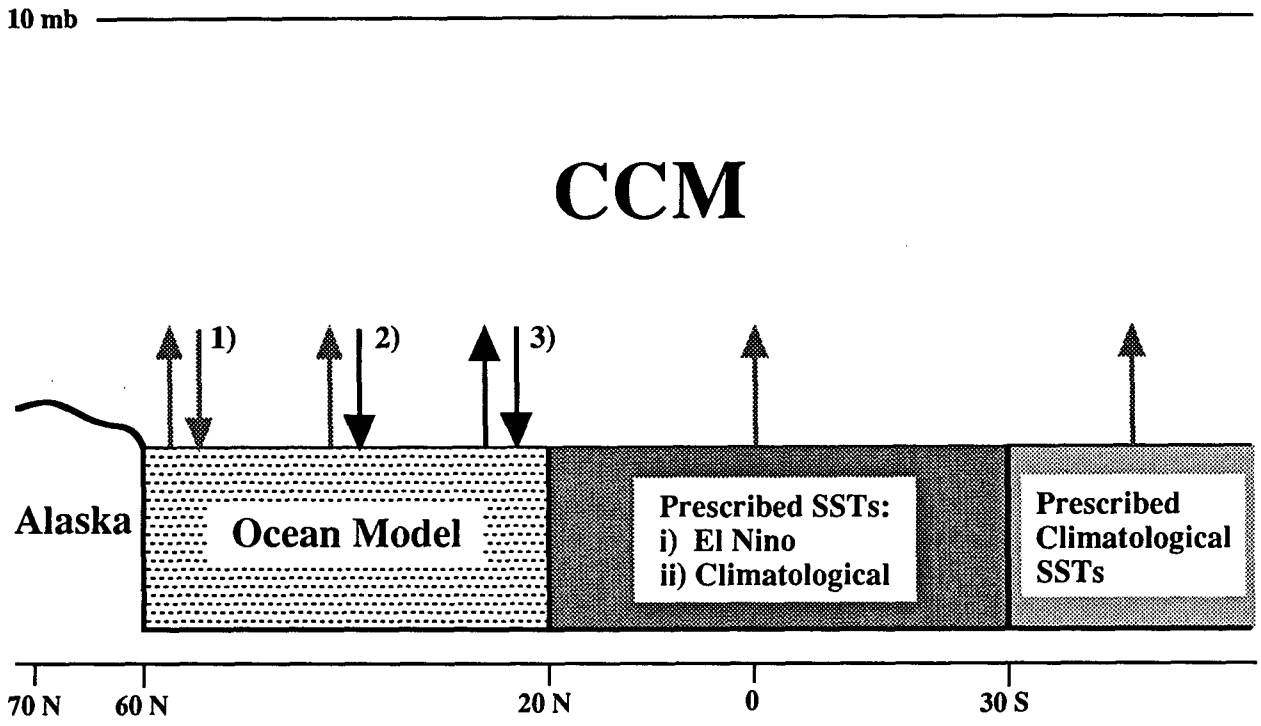

FIG. 4. Cross section through the atmosphere/ocean model system at approximately 170°W. Lightly shaded arrows indicate fluxes computed with prescribed SSTs, and solid arrows indicate fluxes computed with ocean model temperatures. The North Pacific Ocean model is 1) uncoupled (one-way forced), 2) partially coupled, or 3) fully coupled to the CCM.

3. Experiments

Three sensitivity studies (section 4) are used to investigate anomalies over the North Pacific, where anomalies are obtained from the difference between the CCM/ocean model values in the El Niño and climatological simulations. The three sensitivity studies examine (i) the feedback between SST and surface flux anomalies by comparing uncoupled and partially coupled runs, (ii) the feedback between SST and entrainment anomalies by setting entrainment to zero and prescribing the mixed-layer depth, and (iii) the relative impact of entrainment and Ekman pumping on mixed-layer depth anomalies. The results from these analyses will be used to interpret the more complex interactions in the air–sea interaction analysis (section 5), which utilizes fully coupled simulations. The experiments and the associated model simulations are summarized in Table 1.

The El Niño and climatological model simulations are performed in sets of five in order to estimate the statistical significance of the response. The simulations within each set differ only by their initial atmospheric states; the same boundary values and oceanic initial conditions are used in all five runs. The atmospheric variables are initialized with values for a particular day, which are obtained from five different years of Chervin's (1986) 20-year climatological integration. The North Pacific Ocean model is initialized with a six-year average of conditions on 1 June derived from an extended ocean model integration. The simulations span nine months, beginning in June and ending the following February. After a three-month spinup period the ensemble-averaged anomaly fields are presented for September–October–November (SON) and December–January–February (DJF) when the midlatitude response to tropical SST anomalies is largest (Horel and Wallace 1981; Reynolds and Rasmusson 1983; Cayan 1990).

Different sets of CCM/North Pacific Ocean model simulations are used in the sensitivity and the air–sea interaction analyses. In the three sensitivity studies, the CCM fields used to drive the North Pacific Ocean model are obtained from five El Niño runs performed by Aragão (1986) or from five different years of a 20-year climate integration (Chervin 1986). The surface fluxes used to drive the ocean model are smoothed over space and time (Table 1). In the air–sea interaction analysis, a set of fully coupled runs that we performed was to be compared to the one-way forced simulations previously described. However, an exact comparison was not possible due to the addition of a mass-conserving scheme to the CCMOA since 1986 (Chervin, personal communication). In addition, Aragão prescribed El Niño conditions between 30°S and 30°N, which overlaps the ocean model domain be-

TABLE 1. Summary of the experiments and their attributes that are (a) different and (b) the same in the sensitivity studies and the air–sea interaction analysis. The entrainment rate is denoted by w_e, the mixed-layer depth by h, Ekman pumping by w_{ek}, and RC denotes Rasmusson and Carpenter (1982).

(a) Attributes	Sensitivity studies	Air–sea interaction analysis
Experiment (method)	1) SST–surface flux feedback (partially coupled vs uncoupled) 2) SST–entrainment feedback (uncoupled runs: w_e and h predicted vs uncoupled runs: $w_e = 0$, h specified) 3) role of Ekman pumping (w_e vs w_{ek} in uncoupled runs)	1) Atmosphere–ocean communication (uncoupled vs fully coupled)
El Niño SST domain	30°N–30°S in the Pacific	20°N–30°S in the Pacific
El Niño runs	from Aragão (1986)	reintegration of Aragão's runs (1990)
Climate runs	periods of Chervin's (1986) 20-year run	independent climate runs (1990)
Time averaging	2 per day from CCM history tapes	48 times per CCM day
Temporal smoothing	1–2–1 smoothing of surface fluxes	none
Spatial smoothing	9-point smoothing of surface fluxes	none
CCM mass conservation	No	Yes

(b) Attributes	
Anomalies	composite of five El Niño runs minus a corresponding set of five climate runs
SSTs El Niño runs	2 × RC composite in the tropical Pacific, specified to evolve the same in all runs
SSTs climate runs	climatological SSTs in the tropical Pacific, specified to evolve the same in all runs
length of runs	nine months: June–February
CCM initial conditions	Five days from different years of Chervin's 20-year climate run; the same values are used to initialize each of the five corresponding El Niño and climate runs
ocean initial conditions	long-term average of conditions on 1 June, same for all runs

tween 20°N and 30°N. Thus, we have reintegrated the uncoupled simulations so that the differences between the coupled and uncoupled runs result solely from the effects of air–sea interaction. In these simulations surface fluxes are calculated using the method described by Washington and VerPlank (1986); the atmosphere-to-ocean fluxes are averaged over the 48 time steps in one CCM day, during which SST values are held constant, while the ocean-to-atmosphere fluxes are computed at each 30-min CCM time step.

4. Sensitivity studies: Feedback analysis and mixed-layer processes

a. SST–surface flux feedback

Anomalies in the mixed-layer temperature, computed using the uncoupled method and the partially coupled method, are shown in Figs. 5 and 6, respectively. The only difference between the methods (see section 2e) is that T_m affects the surface fluxes in the partially coupled case. In both cases anomalously cold water is found in the central and west Pacific and warm water is located in the Gulf of Alaska and to the west of Mexico during fall (SON) and winter (DJF). This pattern closely resembles the observed anomaly field in the North Pacific during El Niño (MAA). The ocean temperature anomalies in the partially coupled case are $\sim\frac{1}{2}$ to $\frac{2}{3}$ as large as the anomalies in the one-way forced case, indicating a strong negative feedback between Q'_0 and T'_o (where primes denote anomalies). For example, in the northwest Pacific during SON, T'_m is less than -1.8°C in the uncoupled case and -0.9°C in the partially coupled case. The damping of $|T'_m|$ can be understood by examining (8) and (9), the equations used to compute the sensible and latent heat flux. As a warm (cold) T_m anomaly develops, Q_{sh} increases (decreases), which in turn acts to cool (warm) the ocean. There is also a negative feedback between T'_o and Q'_{lh} as the saturation vapor pressure is depen-

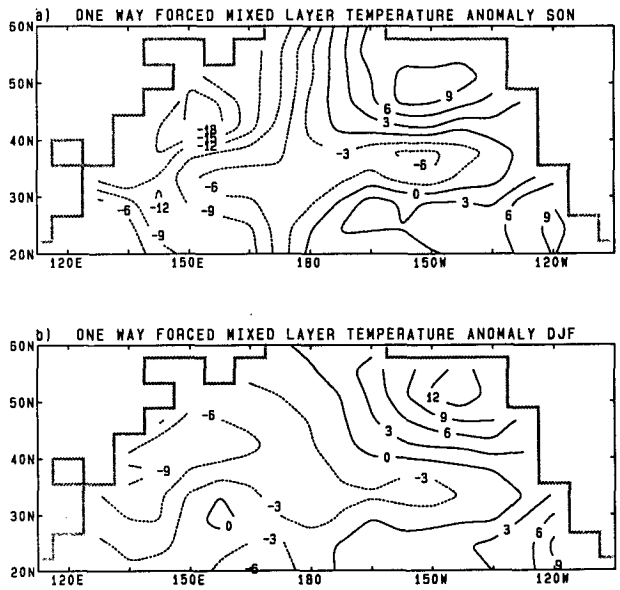

FIG. 5. The mixed-layer temperature anomaly (°C × 10) averaged over (a) SON and (b) DJF. The CCMOA and North Pacific Ocean model are connected using the one-way forced method (section 2d). The anomaly values are obtained by compositing the five El Niño and five climatological simulations and then subtracting the climatological from the El Niño composite.

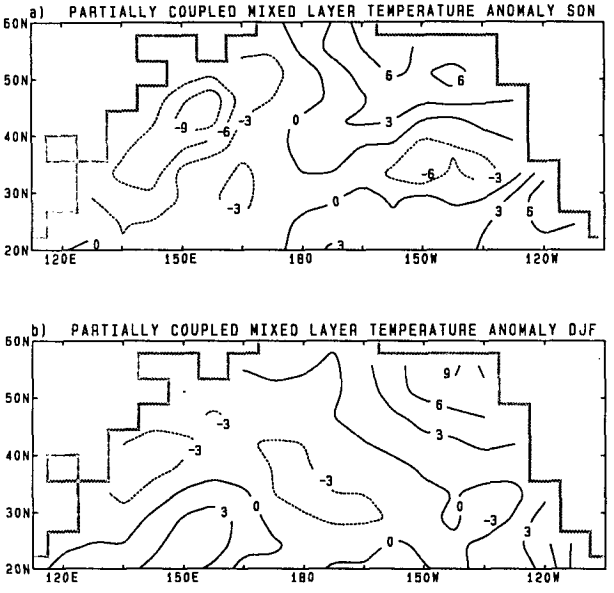

FIG. 6. The partially coupled mixed-layer temperature anomaly (°C × 10) for (a) SON and (b) DJF.

dent on T_o. An increase (decrease) in T_o leads to more (less) evaporation that in turn cools (warms) the ocean. Differences in T'_m between the two cases can also arise from variations in entrainment and other oceanic processes.

The anomalous total surface energy fluxes for the one-way forced and partially coupled case are shown in Figs. 7 and 8, respectively; Q'_0 (positive downward) and T'_o are consistent: the ocean loses heat in the central and west Pacific and gains heat in the eastern Pacific. Not surprisingly, computing the surface fluxes with the same atmospheric variables results in similar Q_0 anomaly patterns in the two cases. The magnitude of Q'_0 is damped in the partially coupled runs; for example, the negative anomaly in the central Pacific during DJF has a maximum value of -40 W m^{-2} in the uncoupled case and -20 W m^{-2} in the partially coupled case. The amount of damping varies with season and location but is generally between 20% and 50%. The reduced T_m and Q_0 anomalies in the partially coupled simulations support the statistical–dynamical model of Frankignoul and Hasselman (1977) in which the midlatitude SST anomaly tendency can be estimated from the anomalous atmospheric forcing and linear damping proportional to the temperature anomaly.

b. *SST–entrainment feedback*

The influence of entrainment on SST anomalies is examined using model simulations in which w_e is set to zero and the mixed-layer depth is prescribed at each grid point. The prescribed depths are obtained by fitting a cubic spline to monthly averaged values of h that are obtained from a composite of the five uncoupled climatological simulations. The T_m anomalies from the prescribed depth simulations are shown in Fig. 9. Comparing Fig. 9 with Fig. 5 indicates that entrainment did not alter the anomaly pattern but it significantly damped the temperature anomalies. The winter T'_m values without entrainment exceed 2.5°C in the northeast Pacific and are less than -3.5°C in the western Pacific, a doubling of the warm anomaly and a fourfold increase in magnitude of the cold anomaly.

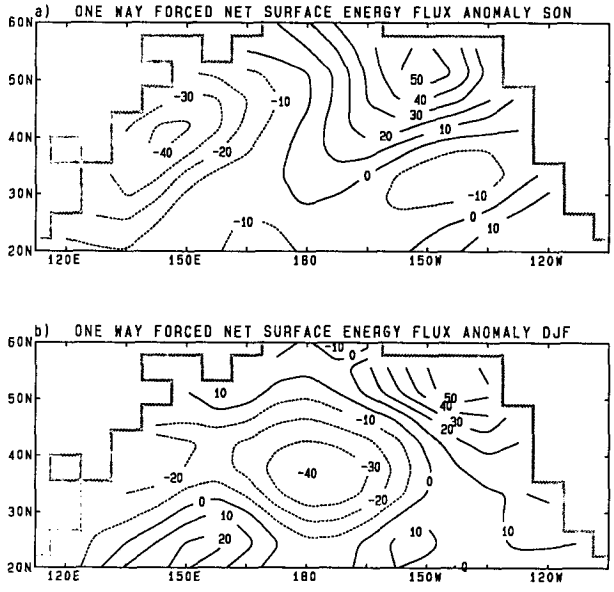

FIG. 7. The one-way forced net surface energy flux anomaly (W m^{-2}) for (a) SON and (b) DJF.

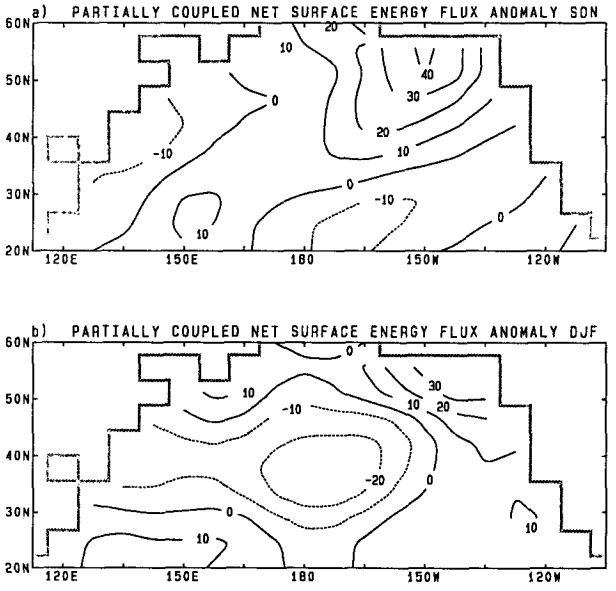

FIG. 8. The partially coupled surface energy flux anomaly (W m^{-2}) for (a) SON and (b) DJF.

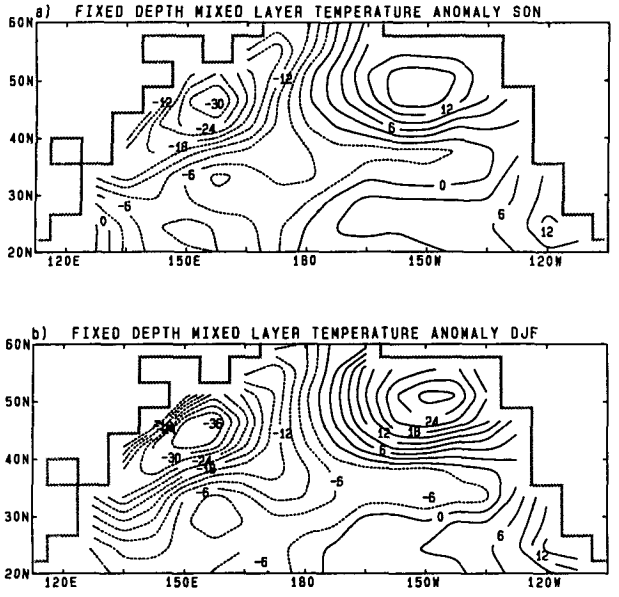

FIG. 9. The mixed-layer temperature anomaly (°C × 10) for (a) SON and (b) DJF, obtained from one-way forced simulations in which seasonally varying mixed-layer depths are prescribed and entrainment is set equal to zero.

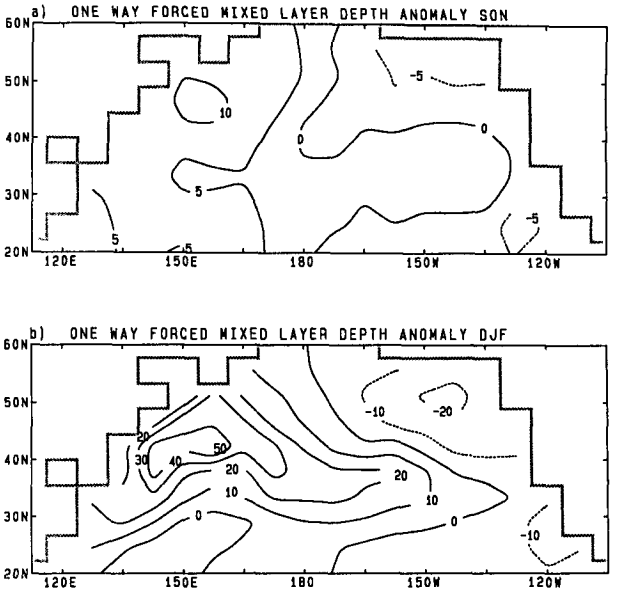

FIG. 10. The one-way forced mixed layer-depth anomaly (m) for (a) SON and (b) DJF.

The negative feedback between w_e and SSTs and the difference in the strength of the feedback between cold and warm anomalies can be understood by examining the anomalous temperature tendency caused by entrainment, $\{(w_e/h)(T_b - T_m)\}'$. Entrainment and the mixed-layer depth are always greater than or equal to zero, and anomalies in T_b are usually small compared with those in the mixed layer, $(T_b - T_m)' \approx -T'_m$. Thus, the anomalous temperature tendency that results from entrainment is generally opposite in sign to T'_m, a negative feedback.

Entrainment also influences the temperature tendency by changing the depth over which the surface forcing is distributed. In the one-way forced runs, w'_e results in positive mixed-layer depth anomalies east of Japan (Fig. 10) where $T'_m < 0$ and negative anomalies in the Gulf of Alaska where $T'_m > 0$. The magnitude of h' is on the order of 5 to 10 m in fall and 20 to 50 m in winter, roughly one-fourth of the model's climatological values (MAA, Fig. 3). In regions where h' is positive (negative) the anomalous surface heating is distributed over a greater (smaller) depth, which also acts to reduce (strengthen) the negative w_e–SST feedback in the northeast (west) Pacific.

In certain situations, entrainment can cause mixed-layer temperature anomalies to form or enhance their development. As discussed in MAA, w_e helps to maintain a cold anomaly in the vicinity of 30°N and the date line during winter. In this region strong wind stirring in the El Niño simulations leads to increased entrainment of the normally cold pycnocline water. In addition, SSTs may be influenced by the entrainment of subsurface temperature anomalies created by horizontal advection or other dynamical processes that are not included in the North Pacific Ocean model.

c. *Ekman pumping*

Mixed-layer depth anomalies due to Ekman pumping are shown in Fig. 11. Anomalies of w_{ek} are less than 3 m month^{-1} over the entire domain, an order of magnitude smaller than w'_e (not shown) and h' (Fig. 10).

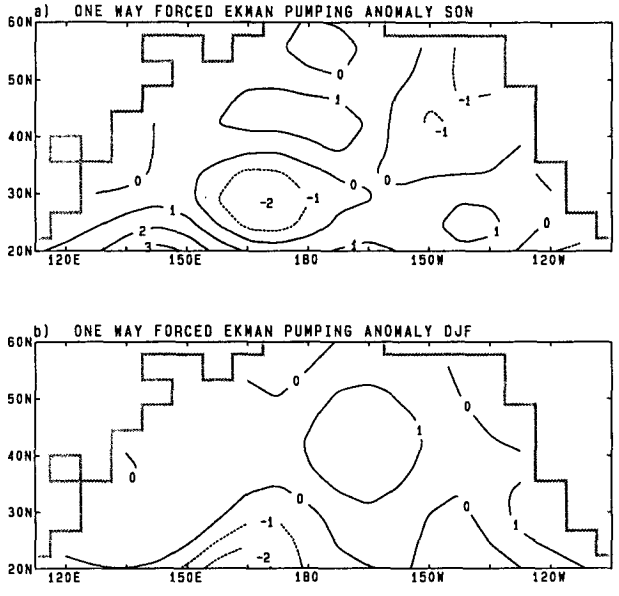

FIG. 11. The one-way forced Ekman pumping anomaly (m month^{-1}) for (a) SON and (b) DJF.

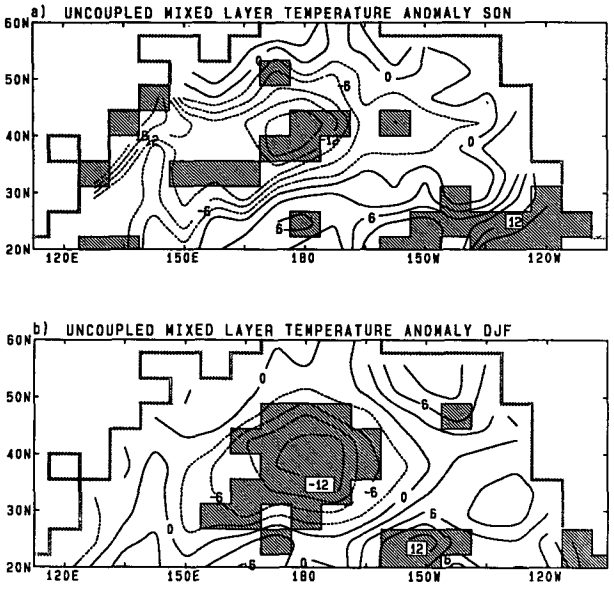

FIG. 12. The mixed-layer temperature anomaly (°C × 10) for (a) SON and (b) DJF. The CCM and North Pacific ocean model are uncoupled. (Note that this figure and the figures from uncoupled simulations that follow are obtained from a reintegrated set of CCM simulations and therefore differ from the original one-way forced figures.) The grid squares where the El Niño and climatological runs are significantly different at the 5% level as determined by a two-sided t test are indicated by shaded boxes.

This indicates that the development of large anomalies in mixed-layer depth during fall and winter are primarily caused by entrainment, which supports the previous results of White (1978), White et al. (1980), Haney et al. (1983), and Frankignoul (1985).

5. Air–sea interaction analysis

The influence of air–sea interaction on the development of ocean anomalies in the North Pacific is assessed by comparing anomalies from the uncoupled and (fully) coupled simulations. The mixed-layer temperature anomaly pattern, associated with changes in the atmospheric circulation during El Niño, are similar in the uncoupled (Fig. 12) and coupled (Fig. 13) runs. In both cases, negative anomalies cover the central Pacific and positive anomalies are located along most of the west coast of North America and in the southwest part of the domain. However, there are differences between the two cases; for example, warm anomalies are found over more of the Pacific between 20°N and 30°N in the uncoupled than in the coupled runs.

While air–sea interaction only slightly altered the anomaly pattern, it significantly reduced the amplitude of the anomalies; comparing Figs. 12 and 13 shows that coupling reduced $|T'_m|$ in the central Pacific from −1.5°C to −0.9°C in fall and from −1.2°C to −0.6°C in winter. In general, the anomalies in the coupled composite are approximately 25% to 50% smaller than in the uncoupled composite. The damping in the fully coupled case primarily results from the negative feedback between T'_m and Q'_0 as suggested by the partially coupled simulations (section 4a).

The relationship between the coupled and uncoupled case becomes more complex when season and location are considered. For example, the SON T_m anomaly is slightly larger in the northeast Pacific in the coupled run, while the anomaly located at 150°W between 20°N and 28°N is over 1.0°C warmer in the uncoupled run during both SON and DJF. Several processes may contribute to regional anomalies that appear in only one set of runs. For example, the large positive anomaly in the southeast Pacific in the uncoupled run results from positive surface flux anomalies in both fall and winter and from a small area of anomalous heating due to entrainment.

Both the coupled and uncoupled North Pacific SST anomaly fields closely resemble the observed DJF anomaly pattern (Fig. 1). The magnitude of the observed DJF anomaly in the central Pacific is −0.9°C, in between the coupled and uncoupled response, while both the data and the coupled case show a maximum SST′ value of 0.6°C in the northeast Pacific. However, comparing Figs. 12 and 13 with Fig. 1 implicitly assumes that the CCM response to a doubling of the tropical SST anomalies is similar to the changes in the real atmosphere between El Niño and La Niña events.

The statistical significance of the difference between the model fields is assessed from the two-sided t statistic (Chervin and Schneider 1976). The t statistic is calculated at each model grid point using a combined

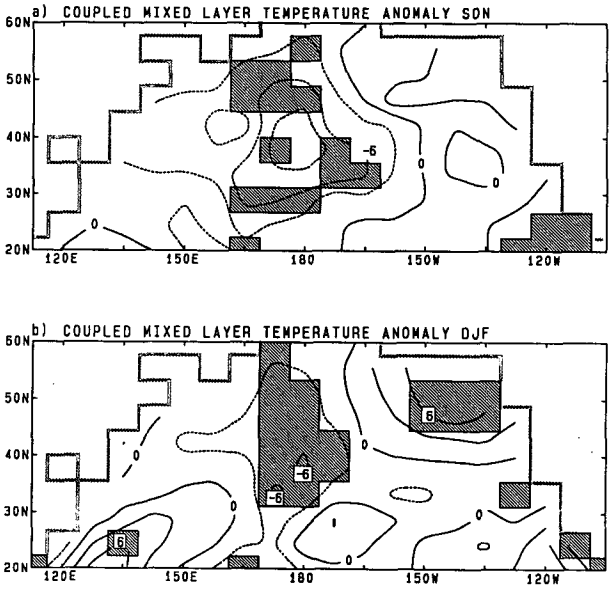

FIG. 13. The mixed-layer temperature anomaly (°C × 10) for (a) SON and (b) DJF. The CCM and North Pacific Ocean model are fully coupled. Grid squares where the t statistic is significant at the 5% level are shaded.

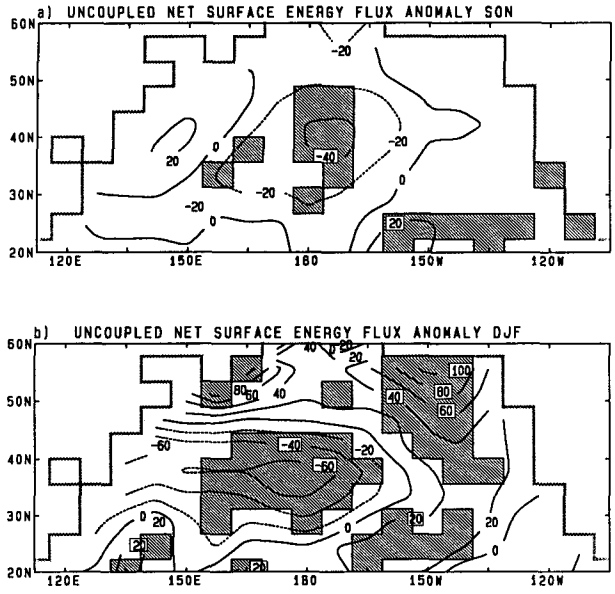

FIG. 14. The uncoupled surface energy flux anomaly (W m^{-2}) for (a) SON and (b) DJF. Grid squares where the t statistic is significant at the 5% level are shaded.

estimate of the variance from the five simulations within each set. The grid squares in which the mixed-layer temperature t statistic values are significant at the 5% level are shaded in Figs. 12 and 13. Large sections of the cold anomaly in the central Pacific are statistically significant during fall and winter in both the coupled and uncoupled cases. Although the mixed-layer temperature anomalies are generally smaller in the coupled runs, there are still a large number of significant grid squares, as air–sea interaction also reduces the T'_m variability (not shown). The variance of T'_m is three to five times larger in the uncoupled simulations.

The T_m anomalies in the original one-way forced set computed using Aragão's (1986) CCM surface fields (Fig. 5) and the anomalies from the reintegration of this set (Fig. 12) are broadly similar in that they both have positive anomalies in the east Pacific and negative anomalies in the central Pacific. If the reintegrated model simulations are treated as an independent set (the differences between the two sets are discussed in section 3), they confirm the statistical significance of the El Niño–induced North Pacific SST anomalies. However, the anomalies near the date line are stronger in the reintegrated set, while the anomalies in the northeast Pacific are larger in the original set. As discussed in Part II, a stronger and more zonally elongated Aleutian Low develops in the reintegrated set compared with Aragão's original simulations.

The uncoupled (Fig. 14) and coupled (Fig. 15) flux anomaly centers are positioned at nearly the same location in the two cases during DJF when Q'_0 is large. The magnitude of the two positive anomaly centers located at about 55°N and the negative center in the vicinity of the date line between 25° and 45°N have been damped by 20% to 40% in the coupled runs during winter. For example, the DJF flux anomalies in the Gulf of Alaska are reduced from 100 to 60 W m^{-2}. The magnitude of Q'_0 was damped by a similar amount in the SST–surface flux feedback analysis (section 4a) where T_o was variable but the atmospheric fields were fixed. Additional processes in the fully coupled simulations also influence Q'_0. As discussed by Frankignoul (1985), anomalous fluxes of heat and moisture into the atmosphere over an SST anomaly reduce $(T_o - T_a)'$ and $(q_s - q_a)'$, which limits the magnitude of Q'_{sh}, Q'_{lh}, and Q'_{lw}. The developing midlatitude SST anomalies also cause changes in the atmospheric circulation, which in turn affects the surface fluxes over the North Pacific (Part II).

The predominance of large-scale atmospheric forcing and the absence of horizontal processes in the North Pacific Ocean model result in a close correspondence between the surface flux and ocean temperature anomaly fields. However, T'_m and Q'_0 do not always vary in unison. For example, in both the coupled and uncoupled runs large values of T'_m develop in the northeast Pacific and not in the northwest Pacific during winter even though Q'_0 is large in both regions. The anomalous temperature tendency due to surface flux anomalies is given by $Q'_0/\rho c\bar{h}$. The monthly DJF values of Q'_0 and $\bar{h}$ for the coupled case are shown in Figs. 16 and 17, respectively. The fluxes are negative in the northwest Pacific in December when the mixed layer is relatively shallow. Very large positive flux anomalies ($Q'_0 > 125$ W m^{-2}) occur in this region when the mixed layer is deep ($\bar{h} > 160$ m). Thus, there is little net

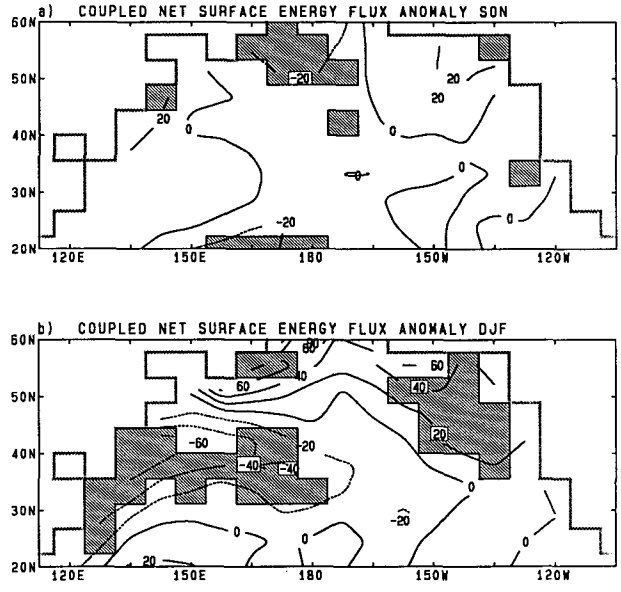

FIG. 15. The coupled surface energy flux anomaly (W m^{-2}) for (a) SON and (b) DJF. Grid squares where the t statistic is significant at the 5% level are shaded.

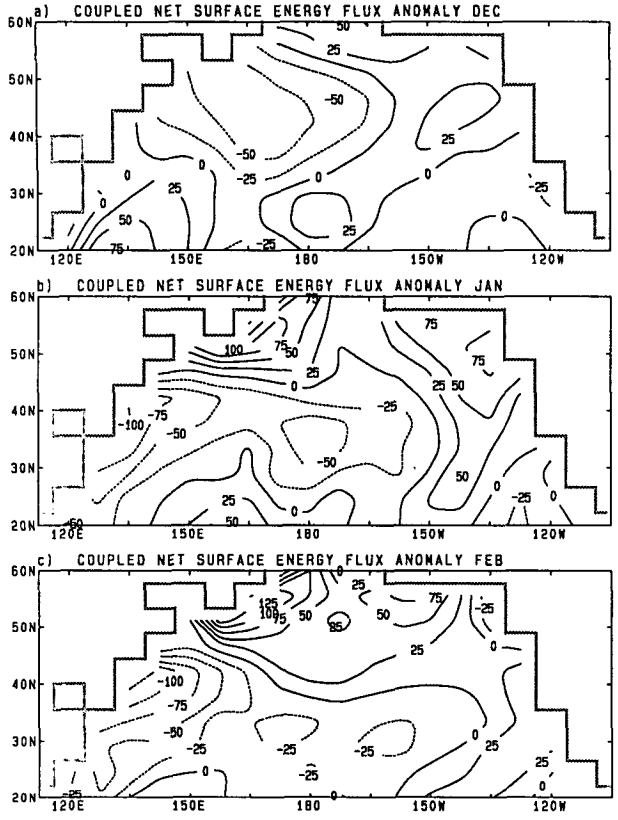

FIG. 16. The coupled surface energy flux anomaly (W m^{-2}) for (a) December, (b) January, (c) February.

change in the seasonal temperature anomaly in the northwest Pacific as the mixed layer is cooled relatively efficiently in December and then warms slowly during January and February. The Q_0 anomaly is positive in all three months over most of the northeast Pacific where $\bar{h} < 140$ m, causing a steady increase in T'_m. These results highlight that both time of year and location can influence the development and maintenance of SST anomalies.

The mixed-layer depth anomaly pattern is similar in the coupled and uncoupled runs (not shown); h' is positive below the anomalous cold SSTs in the central Pacific and negative under the warm SSTs in the east Pacific. However, air–sea interaction substantially reduced the magnitude of the anomalies. The damping is strongest in the central Pacific where h' has a maximum value of approximately 80 m in the uncoupled case and 30 m in the coupled case. In the coupled case there is generally less surface bouyancy forcing as a result of smaller $|Q'_0|$ [Eq. (4)] and a more stable density profile, which both act to reduce the magnitude of w'_e and thus h' [Eq. (3)].

6. Summary and conclusions

We conducted several atmosphere–ocean modeling experiments to study the development of anomalies in the North Pacific Ocean during El Niño. A comparison between simulations in which the NCAR Community Climate Model and a mixed-layer model of the North Pacific Ocean were coupled and uncoupled (CCM surface fluxes were used to drive the ocean model) indicated that air–sea interaction primarily acts to damp ocean anomalies. Anomalies in the ocean temperature and mixed-layer depth had similar patterns in the coupled and uncoupled runs, but the magnitude of the anomalies were generally ½ to ¾ as large in the coupled simulations. Air–sea interaction also decreased the anomaly variance, and as a result, large sections of the SST anomaly field were statistically significant in the coupled runs even though the magnitude of the anomalies was reduced.

Three sensitivity studies provided insight into how air–sea interaction, entrainment, and Ekman pumping influenced the development of ocean anomalies in the coupled runs. In the first study, simulations using the partially coupled and uncoupled methods were compared; the only difference between the methods was that mixed-layer temperatures affect the surface fluxes in the partially coupled case. The ocean temperature anomalies were substantially reduced in the partially coupled simulations, suggesting a strong negative feedback between the surface flux and SST anomalies. The flux anomalies were diminished by ~20% to 50% in

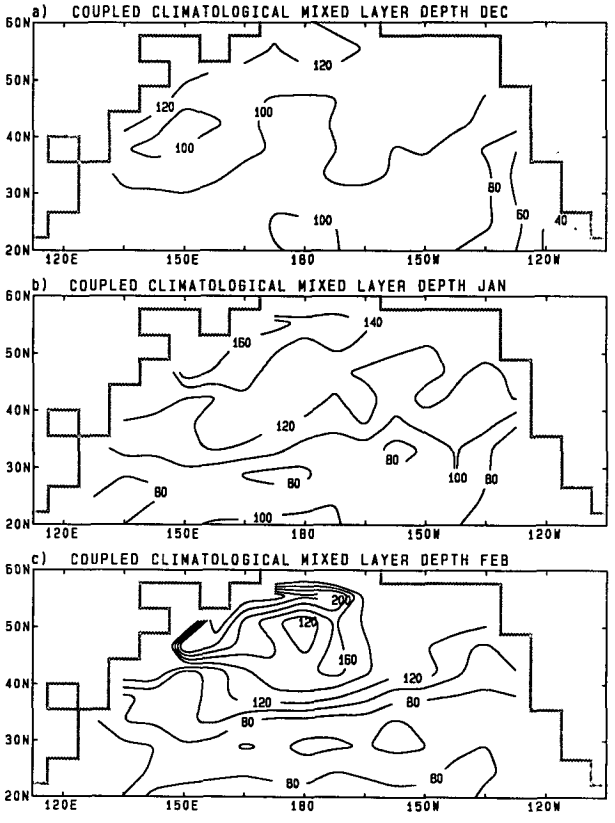

FIG. 17. The coupled climatological mixed-layer depth (m) for (a) December, (b) January, (c) February.

the partially coupled case and by a similar amount in the fully interactive case. The second sensitivity study, which utilized simulations with prescribed mixed-layer depths, indicated that entrainment often strongly damps SST anomalies. Entrainment of relatively warm (cold) water from beneath the mixed layer usually occurred when the mixed layer was cold (warm). Entrainment also influenced SST anomalies by changing the mixed-layer depth. In the west Pacific, the surface forcing was distributed over a greater depth in the El Niño runs, which further damped the SST anomalies. The third sensitivity analysis suggested that Ekman pumping in the open ocean has a negligible effect on the development of midlatitude mixed-layer depth anomalies.

Air–sea interaction and entrainment, while generally suppressing ocean anomalies, occasionally helped to generate or enhance SST anomalies. Changes in the atmospheric circulation in response to midlatitude SST anomalies (see Part II) resulted in stronger downward surface fluxes in the northeast Pacific during fall in the coupled runs, which in turn enhanced the development of the warm SST anomaly in the Gulf of Alaska. In addition, evolution of SST anomalies depends on the time of year and location. The SST anomalies that form in the late fall or early winter when the surface forcing strengthens are likely to remain through the winter due to the large thermal inertia of the mixed layer.

Our findings are contingent on several factors, including the simplicity of the ocean model, the parameterizations used to compute the surface fluxes, and the CCM response to prescribed SST anomalies in the tropical Pacific. In addition, it was necessary to apply large correction values to the surface flux fields over the North Pacific Ocean in order to simulate realistic climatological SSTs. With these limitations in mind, the results from this paper and MAA suggest that the anomalously cold water in the central Pacific and warm water along the coast of North America that form during El Niño result from the atmosphere forcing the ocean. Including air–sea feedback in the North Pacific resulted in smaller SST anomalies. The influence of these anomalies on the near-surface atmospheric fields, storm tracks, and hemispheric circulation is investigated in Part II of this study.

Acknowledgments. This work comprised part of my Ph.D. research at the University of Wisconsin. I wish to thank Dr. John Kutzbach, my Ph.D. advisor, for his support and guidance. Dr. Robert Chervin of the National Center for Atmospheric Research (NCAR) provided model history tapes and a multitasked version of the Community Climate Model. The scientific input and comments from Drs. David Battisti, Robert Gallimore, Martin Hoerling, and Klaus Weickmann are greatly appreciated. Arthur Miller, Robert Livezey, and an anonymous reviewer suggested several improvements to the manuscript. Rich Selin and Pat Behling helped to draft the figures.

This research project was supported under Grant ATM89-02849 from the National Science Foundation's Climate Dynamics program to the University of Wisconsin–Madison. Additional support for the author and part of the publication costs were provided by a CIRES fellowship at the University of Colorado. The computations were made at NCAR, which is sponsored by the National Science Foundation, with Grant 35381044 from the NCAR Scientific Computing Division.

APPENDIX

The Temperature below the Mixed Layer (T_b)

The first step in computing T_b is to determine $\hat{h}$, the distance between the base of the mixed layer and the bottom of L, the layer of the convective–diffusive (C–D) model in which the base of the mixed layer resides,

$$\hat{h} = \sum_{k=1}^{L} \Delta z_k - h. \tag{A1}$$

The temperature of layer $\hat{h}$ is

$$\hat{T} = \sum_{k=1}^{L} \frac{T_k \Delta z_k - T_m h}{\hat{h}} \quad \text{for} \quad \hat{h} \geq 2 \text{ m}$$

or

$$\hat{T} = T_m - \frac{1}{2}(T_m - T_{k+1}) \quad \text{for} \quad \hat{h} < 2 \text{ m}, \tag{A2}$$

and a layer average temperature is also computed according to

$$T_{L+1/2} = \frac{T_L + T_{L+1}}{2} \quad \text{for} \quad L = 1, 2, 3$$

or

$$T_{L+1/2} = T_L \quad \text{for} \quad L = 4. \tag{A3}$$

Heald and Kim (1979) present a number of empirical formulas for computing T_b; we use $T_b = \hat{T}$ with the constraint that $\hat{T} > T_{L+1/2}$. Here $\hat{T}$ is chosen so that the heat content of $h + \hat{h}$ and the C–D model through layer L are equivalent (see Fig. 3). If $\rho_m > \hat{\rho}$, then T_m and $\hat{T}$ are convectively mixed. The temperature of all C–D model layers that are completely within the mixed layer are reset to T_m, and a new value of T_L is computed in order to conserve heat in both models. A similar set of equations is used to obtain S_b.

REFERENCES

Alexander, M. A., 1990: Simulation of the response of the North Pacific Ocean to the anomalous atmospheric circulation associated with El Niño. *Climate Dyn.*, **5**, 53–65.

——, 1992: Midlatitude air–sea interaction during El Niño. Part II: The Northern Hemisphere atmosphere. *J. Climate*, **5**, 959–972.

Alexander, R. C., and R. L. Mobley, 1976: Monthly average sea-

surface temperature and ice-pack limits in a 1° global grid. *Mon. Wea. Rev.*, **104,** 143–148.

Aragão, J. O. R., 1986: A general circulation model investigation of the atmospheric response to El Niño. Cooperative thesis No. 100, University of Miami and National Center for Atmospheric Research, 144 pp.

Bjerknes, J., 1966: A possible response of the atmospheric Hadley circulation to equatorial anomalies of ocean temperatures. *Tellus,* **18,** 820–829.

——, 1969: Atmospheric teleconnections from the equatorial Pacific. *Mon. Wea. Rev.*, **97,** 163–172.

Blackmon, M. L., J. E. Geisler, and E. J. Pitcher, 1983: A general circulation model study of January climate anomaly patterns associated with interannual variation of equatorial Pacific sea surface temperatures. *J. Atmos. Sci.*, **40,** 1410–1425.

Cayan, D. R., 1980: Large-scale relationships between sea surface temperature and surface air temperature. *Mon. Wea. Rev.*, **9,** 1293–1301.

——, 1990: Variability of latent and sensible heat flux over the oceans. Ph.D. dissertation, University of California, San Diego, 199 pp.

Chervin, R. M., 1986: Interannual variability and seasonal climate predictability. *J. Atmos. Sci.*, **43,** 233–251.

——, and S. H. Schneider, 1976: On determining the statistical significance of climate experiments with general circulation models. *J. Atmos. Sci.*, **33,** 405–412.

Clark, N. E., 1972: Specification of sea surface temperature anomaly patterns in the eastern North Pacific. *J. Phys. Oceanogr.*, **2,** 391–404.

Davis, R. E., 1976: Predictability of sea surface temperature and sea level pressure anomalies over the North Pacific Ocean. *J. Phys. Oceanogr.*, **6,** 249–266.

——, 1978: Predictability of sea level pressure anomalies over the North Pacific Ocean. *J. Phys. Oceanogr.*, **8,** 233–246.

——, R. DeSzoeke, and P. Niiler, 1981: Variability in the upper ocean during MILE. Part II: Modeling the mixed layer response. *Deep-Sea Res.*, **28A,** 1453–1475.

Emery, W. J., 1976: The role of vertical motion in the heat budget of the upper northeastern Pacific Ocean. *J. Phys. Oceanogr.*, **6,** 299–305.

——, and K. Hamilton, 1985: Atmospheric forcing of interannual variability in the northeast Pacific Ocean: Connections with El Niño. *J. Geophys. Res.*, **90,** 857–868.

Enfield, D. B., and J. S. Allen, 1980: On the structure and dynamics of monthly mean sea level anomalies along the Pacific Coast of North and South America. *J. Phys. Oceanogr.*, **10,** 557–588.

Frankignoul, C., 1985: Sea surface temperature anomalies, planetary waves, and air–sea feedback in the middle latitudes. *Rev. Geophys.*, **23,** 357–390.

——, and K. Hasselmann, 1977: Stochastic climate models. Part 2: Application to sea-surface temperature anomalies and thermocline variability. *Tellus,* **29,** 289–305.

——, and R. W. Reynolds, 1983: Testing a dynamical model for midlatitude sea surface temperature anomalies. *J. Phys. Oceanogr.*, **13,** 1131–1145.

Geisler, J. E., M. L. Blackmon, G. T. Bates, and S. Muñoz, 1985: Sensitivity of January climate response to the magnitude and position of equatorial Pacific sea-surface temperature anomalies. *J. Atmos. Sci.*, **42,** 1037–1049.

Gill, A. E., and P. P. Niiler, 1973: The theory of the seasonal variability in the ocean. *Deep-Sea Res.*, **20,** 141–177.

Hanawa, K., Y. Yoshikawa, and T. Watanabe, 1989: Composite analyses of wintertime wind stress vector fields with respect to SST anomalies in the western North Pacific and the ENSO events Part II. ENSO composite. *J. Meteor. Soc. Japan,* **65,** 833–845.

Haney, R. L., 1980: A numerical case study of the development of large-scale thermal anomalies in the central North Pacific Ocean. *J. Phys. Oceanogr.*, **10,** 541–556.

——, 1985: Midlatitude sea surface temperature anomalies: A numerical hindcast. *J. Phys. Oceanogr.*, **15,** 787–799.

——, B. H. Houtman, and W. H. Little, 1983: The relationship between wind and sea surface temperature anomalies in the midlatitude North Pacific Ocean. *Atmos.–Ocean,* **21,** 168–186.

Heald, R. C., and J.-W. Kim, 1979: Parameterization of the oceanic mixed layer for use in general circulation models. Department of Atmospheric Science and Climatic Research Institute, Oregon State University, Corvalis, Report No. 10, 48 pp.

Horel, J. D., and J. M. Wallace, 1981: Planetary-scale atmospheric phenomena associated with the Southern Oscillation. *Mon. Wea. Rev.*, **109,** 813–829.

Johnson, M. A., and J. J. O'Brien, 1990: The northeast Pacific Ocean response to the 1982–1983 El Niño. *J. Geophys. Res.*, **95,** 7155–7166.

Lau, N.-C., and M. J. Nath, 1990: A general circulation model study of the atmospheric response to extratropical SST anomalies observed in 1950–79. *J. Climate,* **3,** 965–989.

Lanzante, J. R., 1984: A rotated eigenanalysis of the correlation between 700 mb heights and sea surface temperatures in the Pacific and Atlantic. *Mon. Wea. Rev.*, **112,** 2270–2280.

Luksch, U., H. v. Storch, and E. Maier-Reimer, 1990: Modeling North Pacific SST anomalies as a response to anomalous atmospheric forcing. *J. Mar. Syst.*, **1,** 51–60.

Manabe, S., and R. J. Stouffer, 1988: Two stable equilibria of a coupled ocean–atmosphere model. *J. Climate,* **1,** 841–866.

Mysak, L. A., 1986: El Niño, interannual variability and fisheries in the northeast Pacific. *Ocean. Can. J. Fish. Aquat. Sci.*, **43,** 464–497.

Namias, J., 1959: Recent seasonal interactions between North Pacific waters and the overlying atmospheric circulation. *J. Geophys. Res.*, **64,** 631–646.

——, 1965: Macroscopic association between mean monthly sea surface temperature and the overlying winds. *J. Geophys. Res.*, **70,** 2307–2318.

——, 1972: Experiments in objectively predicting some atmospheric and oceanic variables for the winter of 1971-1972. *J. Appl. Meteor.*, **11,** 1164–1174.

——, 1973: Thermal communication between the sea surface and the lower troposphere. *J. Phys. Oceanogr.*, **3,** 373–378.

Niebauer, H. J., 1980: Sea ice and temperature variability in the eastern Bering Sea and the relation to atmospheric fluctuations. *J. Geophys. Res.*, **85,** 7507–7515.

Niiler, P. P., and E. B. Kraus, 1977: One-dimensional models of the upper ocean. *Modeling and Prediction of the Upper Layers of the Ocean,* E. B. Kraus, Ed., Pergamon Press, 143–172.

Palmer, T. N., and Z. Sun, 1985: A modelling and observational study of the relationship between sea surface temperature in the north-west Atlantic and the atmospheric general circulation. *Quart. J. Roy. Meteor. Soc.*, **111,** 947–975.

Pan, Y. H., and A. H. Oort, 1983: Global climate variations connected with sea surface temperature anomalies in the eastern equatorial Pacific Ocean for the 1958–73 period. *Mon. Wea. Rev.*, **111,** 1244–1258.

——, and ——, 1990: Correlation analyses between sea surface temperature anomalies in the eastern equatorial Pacific and the world ocean. *Climate Dyn.*, **4,** 191–205.

Paulson, C. A., and J. J. Simpson, 1977: Irradience measurements in the upper ocean. *J. Phys. Oceanogr.*, **7,** 952–956.

Pitcher, E. J., M. L. Blackmon, G. T. Bates, and S. Muñoz, 1988: The effects of North Pacific sea surface temperature anomalies on the January climate of a general circulation model. *J. Atmos. Sci.*, **45,** 173–188.

——, R. C. Malone, V. Ramanathan, M. L. Blackmon, K. Puri, and W. Bourke, 1983: January and July simulations with a spectral general circulation model. *J. Atmos. Sci.*, **40,** 580–604.

Pollard, D., M. L. Batteen, and Y.-J. Han, 1983: Development of a simple upper-ocean and sea-ice model. *J. Phys. Oceanogr.*, **13,** 754–768.

Pollard, R. T., and R. C. Millard, 1970: Comparison between observed and simulated wind-generated inertial oscillations. *Deep-Sea Res.*, **17,** 813–821.

Rasmusson, E. M., and T. H. Carpenter, 1982: Variations in tropical sea surface temperature and surface wind fields associated with

the Southern Oscillation/El Niño events. *Mon. Wea. Rev.*, **110**, 354–384.

Reynolds, R. W., and E. M. Rasmusson, 1983: The North Pacific sea surface temperature associated with El Niño events. *Proc. of the Seventh Annual Climate Diagnostic Workshop*, Boulder, CO, NOAA, 298–310. [NTIS No. PB83-208033.]

Salmon, R., and M. C. Hendershott, 1976: Large-scale air–sea interactions with a simple general circulation model. *Tellus*, **28**, 228–242.

Sausen, R., K. Barthel, and K. Hasselmann, 1988: Coupled ocean–atmosphere models with flux correction. *Climate Dyn.*, **2**, 145–163.

Simonot, J.-Y., and H. L. Le Treut, 1986: Climatological field of mean optical properties of the world ocean. *J. Geophys. Res.*, **91**, 6642–6646.

Wagner, A. J., 1984: Possible mid-latitude atmospheric generation of anomalously warm surface waters in the Gulf of Alaska from autumn 1982 to spring 1983. *Trop. Ocean–Atmos. Newslett.*, **26**, 15–16.

Wallace, J. M., and Q. Jiang, 1987: On the observed structure of the interannual variability of the atmosphere/ocean climate system. *Atmospheric and Oceanic Variability*, H. Cattle, Ed., Roy. Meteor. Soc., 17–43.

——, C. Smith, and Q. Jiang, 1990: Spatial patterns of atmosphere–ocean interaction in the northern winter. *J. Climate*, **3**, 990–998.

Walsh, J. E., and M. B. Richman, 1981: Seasonality in the association between surface temperatures over the United States and the North Pacific Ocean. *Mon. Wea. Rev.*, **109**, 767–783.

Washington, W. M., Ed., 1982: Documentation for the Community Climate Model, CCM: version 0. National Center for Atmospheric Research, Boulder, CO. Unpaginated. [NTIS No. PB82-194192]

——, and L. VerPlank, 1986: A description of coupled general circulation models of the atmosphere and oceans used for carbon dioxide studies. NCAR Tech. Note, NCAR/TN-271+EDD, National Center for Atmospheric Research, Boulder, CO, 29 pp.

Weare, B. C., A. R. Navato, and R. E. Newell, 1976: Empirical orthogonal analysis of Pacific Ocean sea surface temperatures. *J. Phys. Oceanogr.*, **6**, 671–678.

White, W. B., 1978: A wind driven model experiment of the seasonal cycle of the main thermocline in the interior midlatitude of the North Pacific. *J. Phys. Oceanogr.*, **8**, 818–824.

——, R. Bernstein, G. McNally, S. Pazan, and R. Dickson, 1980: The thermocline response to transient atmospheric forcing in the interior midlatitude North Pacific 1976–1978. *J. Phys. Oceanogr.*, **10**, 372–384.

Wright, P. B., 1983: Sea surface temperature fluctuations in the Pacific, 0°–50°N. *Trop. Ocean–Atmos. Newslett.*, **19**, 14–15.